HHS Public Access

Author manuscript

J Orthop Res. Author manuscript; available in PMC 2020 April 01.

Published in final edited form as:

J Orthop Res. 2019 April ; 37(4): 845–854. doi:10.1002/jor.24238.

Effect of Interface Mechanical Discontinuities on Scaffold-Cartilage Integration

Supansa Yodmuang[1], **Hongqiang Guo**[1], **Caroline Brial**[2], **Russell F. Warren**[3], **Peter A. Torzilli**[1], **Tony Chen**[1], **Suzanne A. Maher**[1,2]

[1]Orthopedic Soft Tissue Research Program, Hospital for Special Surgery, New York, New York,

[2]Department of Biomechanics, Hospital for Special Surgery, 535 East 70th Street, New York 10021 New York,

[3]Sports Medicine and Shoulder Service, Hospital for Special Surgery, New York, New York

Abstract

A consistent lack of lateral integration between scaffolds and adjacent articular cartilage has been exhibited in vitro and in vivo. Given the mismatch in mechanical properties between scaffolds and articular cartilage, the mechanical discontinuity that occurs at the interface has been implicated as a key factor, but remains inadequately studied. Our objective was to investigate how the mechanical environment within a mechanically loaded scaffold-cartilage construct might affect integration. We hypothesized that the magnitude of the mechanical discontinuity at the scaffold-cartilage interface would be related to decreased integration. To test this hypothesis, chondrocyte seeded scaffolds were embedded into cartilage explants, pre-cultured for 14 days, and then mechanically loaded for 28 days at either 1N or 6N of applied load. Constructs were kept either peripherally confined or unconfined throughout the duration of the experiment. Stress, strain, fluid flow, and relative displacements at the cartilage-scaffold interface and within the scaffold were quantified using biphasic, inhomogeneous finite element models (bFEMs). The bFEMs indicated compressive and shear stress discontinuities occurred at the scaffold-cartilage interface for the confined and unconfined groups. The mechanical strength of the scaffold-cartilage interface and scaffold GAG content were higher in the radially confined 1N loaded groups. Multivariate regression analyses identified the strength of the interface prior to the commencement of loading and fluid flow within the scaffold as the main factors associated with scaffold-cartilage integration. Our study suggests a minimum level of scaffold-cartilage integration is needed prior to the commencement of loading, although the exact threshold has yet to be identified.

Keywords

biomechanics scaffold-cartilage interface; articular cartilage and mechanical loading

Correspondence to: Suzanne A. Maher (T: 212-606-1083; F: 212-606-1490; mahers@hss.edu).

AUTHOR CONTRIBUTIONS

All authors have read and approved the final submitted manuscript. SY contributed to bioreactor studies and carried out the experiments. HG performed bFEMs. CB contributed to mechanical testing. RW and PT helped with study design, reviewed the data, and manuscript. TC helped to design the bioreactor studies, helped with data interpretation, and ran all statistical analyses. SM contributed to data analysis, interpreted data, and drafted the manuscript. All authors provided critical feedback and helped shape the manuscript.

Hyaline cartilage has unique mechanical and biological characteristics that enable its role in joint function. However, a lack of vascularization, low cell population, and dense extracellular matrix result in an inability to self-repair after injury.[1,2] Localized articular cartilage damage can alter joint function, spread over time to involve the remainder of the joint, and lead to the development of osteoarthritis (OA). Many approaches intended to repair articular cartilage have been developed based on the premise that scaffolds can be engineered to have the capacity to regenerate cartilage-like tissue. The degradation profiles, morphology, and cell-seeding protocols for scaffold-assisted repair approaches can be widely varied, resulting in a design space with almost unlimited possibilities. However, a design that creates a functional and durable repair for articular cartilage defects has not yet emerged.

Ideally, scaffolds for articular cartilage repair should mechanically withstand in vivo loads and integrate with adjacent articular cartilage, to create “lateral integration.” But a consistent lack of lateral integration has been exhibited in vitro and in vivo.[3] Many attempts have been made to address this problem, including the use of enzymatic digestion,[4] growth factor and cytokine release,[5] cell seeding,[6] and the use of adhesion peptides.[7] The feasibility of each approach is most often assessed in static tissue culture models, where the scaffold is inserted into a cartilage explant and the construct is cultured without any mechanical stimulus. Such studies neglect the role that loading might play in the response of the interface; a critical omission in a tissue designed to withstand high applied forces.[8,9] There exists a need for a deeper understanding of the relationship between the mechanical environment at the scaffold-cartilage interface, the biological response of the cells at that interface, and subsequent integration.[10] Bioreactor models offer the opportunity to stimulate the scaffold-cartilage interface response with controlled loads. Computational approaches such as finite element (FE) models are capable of quantifying the stresses, strains, and fluid flow within mechanically loaded tissue and scaffolds.[11,12] By applying FE models to the analysis of bioreactor studies, an opportunity to relate mechanical conditions to cell response arises.

The objective of this study was to investigate how the physical environment within a mechanically loaded scaffold-cartilage construct relates to lateral integration. We hypothesized that the mechanical discontinuity at the scaffold-cartilage interface would be related to decreased scaffold-cartilage integration. To test this hypothesis, we subjected cartilage-scaffold explants to a range of loading conditions by varying applied force and peripheral confinement. Stress, strain, and displacements at the cartilage-scaffold interface and throughout the scaffold were quantified by computational biphasic finite element models (bFEMs). Interface strength, and scaffold collagen, GAG, and DNA content were quantified after 28 days of bioreactor loading. The relationship between the outputs from the computational model and the physical bioreactor model were compared using multivariate regression analyses.

MATERIALS AND METHODS

Preparation of the Scaffolds

To avoid the complexities of modeling the time-varying change in properties of degradable scaffolds, we used non-degradable macroporous poly(vinyl alcohol), PVA, hereafter referred to as "*scaffold*," that was previously developed as a candidate material for cartilage repair.[13] As previously described,[14] surgical gelatin sponges (Ethicon-Johnson & Johnson, Somerville, NJ) were saturated with deionized water and incubated in gradations of 1–10% PVA (M_W ~195,000; Sigma Aldrich, St. Louis, MO) solution in deionized water. The sponges were placed into 100 × 20 mm Petri dish and subjected to six freeze-thaw cycles (−20°C for 20 h followed by 25°C for 4 h). Cylinders were cored out from the frozen sponges using biopsy punch (diameter Ø5 mm) and cut to desired height of 2.5 mm using freezing stage microtome. The cylinders were digested in 400 U/ml collagenase type II (Worthington Biochemical Corp., Lakewood, NJ) for 8 h at 37°C to remove the gelatin sponges. The resulting macroporous PVA scaffolds were washed in deionized water to remove collagenase, washed in 70% ethanol for 20 min, followed by a wash in 100% ethanol for 20 min, and then air-dried in a laminar flow hood.

Isolation of Chondrocytes

Cartilage was harvested from the trochlear grove and femoral condyles of 2 month old calves ($n = 6$) (Max Insel Cohen, Livingston, NJ) dissected into small pieces and then digested for 10 h using collagenase type II (400 U/ml, Worthington Biochemical Corp) in 7.5 ml/g tissue of high glucose DMEM (hgDMEM) supplemented with 5% fetal bovine serum (FBS) and antibiotics. The suspension was filtered through a 70 μm pore size cell strainer and plated at high density of 2.5×10^5 cells/cm^2 in chondrocyte growth medium (hgDMEM supplemented with 10% FBS, 100 U/ml antibiotic-antimycotic (Fisher Scientific, Fair Lawn, NJ)).

Preparation of Scaffold-Cartilage Defect Model

Juvenile bovine cartilage was cored out from the trochlear grove and femoral condyles using a 10 mm diameter "Donor" Harvester (Arthrex Inc, Naples, FL). Superficial and deep zones of cartilage were removed using a custom sectioning device to create uniform cartilage disks 2.5 mm in height. Cylindrical through-thickness defects of 3.5 mm diameter were created at the center of the cartilage disks using a biopsy punch. Dried macroporous PVA scaffolds were placed into the defects and rehydrated with 0.25×10^5 chondrocytes in 50 μl of DMEM pipetted directly onto the scaffold. All explants were maintained in static culture (unloaded conditions) either in unconfined or confined conditions for 28 days. Explants in the confined groups were placed in polydimethylsiloxane (PDMS) rings to simulate the properties of the surrounding cartilage. Chondrogenic medium (Advanced DMEM supplemented with 100 nM dexamethasone, 50 μg/ml ascorbate, and 10 ng/ml TGF-β3[15] was used, with medium changes every 3 days.

Bioreactor Physical Model

After 28 days of static culture, cell-seeded scaffold-cartilage constructs were subjected to either no load (0N) or prescribed sinusoidal loads of 1N (stress = 12.7 kPa) or 6N (stress = 76.4 kPa) at 0.5 Hz for 450 cycles/day, 5 days a week for 2 weeks. Mechanical loading was applied using a Tissue Growth Technologies Cartigen Bioreactor (Minneapolis, MN), into which each construct along with 750 μl of chondrogenic medium was placed. The magnitude of load (0, 1N, and 6N), and peripheral confinement of the cartilage explant (confined, “C” and unconfined “U”) were controlled to result in six groups as follows (Fig. 1): (i) Unconfined, 1N load; (ii) Unconfined, 6N load; (iii) Unconfined, Static (Control); (iv) Confined, 1N load; (v) Confined, 6N load; (vi) Confined Static (Control). $n = 6$ samples per group, per time point for push-out testing and biochemical analyses, which were the primary outcome measures. Histological analyses and microCT were used as secondary outcome metrics and applied to a sub-set of samples. The experiment was run in duplicate.

Integration Testing and Biochemical Analysis

Scaffold-cartilage interface strength was determined using push-out tests ($n = 6$ per group per time point). Using an EnduraTEC ELF 3200 system (Bose, Eden Prairie, MN), a 2.75 mm diameter stainless steel indenter was displaced at a rate of 10 μm/s,[16] and the force throughout testing was recorded. The maximum push-out force was recorded and normalized to the surface area of the inner wall of the cartilage explant, so that the maximum interfacial stress before failure, or *interface strength* could be computed. Interface strength was quantified at D28 (at the end of static culture) and D42 (at the end of bioreactor loading). Values from D28 were used as inputs to the bFEM. The scaffolds were then frozen and stored at −20°C for biochemical testing for glycosaminoglycan (GAG) content via the DMMB assay,[17] hydroxyproline (OHP) content via acid hydrolysis assay,[18] and DNA content via the Picogreen assay (Invitrogen).

Histology and Immunohistochemistry

Due to the technical challenges of processing the porous PVA through histology, a subset of samples was chosen for this analysis. Scaffold-cartilage constructs from the 42D 1N and 6N confined groups were fixed in 4% formaldehyde at 4°C overnight and dehydrated in a graded series of ethanol, embedded in paraffin, and sectioned to 8 μm thick. The sections were dehydrated in water and stained with Safranin O/Fast Green to detect glycosaminoglycans (GAG). For immunostaining of Collagen type II, antigen retrieval was performed by incubating with 0.1% trypsin for 5 min at 37°C. Blocking endogenous peroxidase activity was performed by incubating the sections in 0.3% H_2O_2/methanol for 30 min at room temperature. The sections were incubated with blocking serum (Vectastain ABC, Burlingame, CA) for 30 min at room temperature, rinsed in PBS and incubated overnight at 4°C with 1:100 mouse anti-human IgG collagen type II monoclonal antibody (CIIC1; Developmental Studies Hybridoma Bank, Iowa City, IA). Biotinylated secondary antibody was applied to the sections as described in the manufacture’s protocol followed by signal detection using DAB Peroxidase Substrate Kit (Vectastain ABC, Burlingame, CA). The sections were counterstained with hematoxylin.

Micro-Computed Tomography (μCT)

Micro-computed tomography (μCT) was used to visualize the scaffold-cartilage interface in $n = 3$ samples from the 42D 1N and 6N confined groups. Constructs were soaked in Lugol's solution (5% w/w I_2 and 10% KI in dH_2O) for 24 h and then scanned at 70 kVp with 10 μm voxel size, 0.36° rotation step (180° angular range) and exposure time of 400 ms per view via Scanco μCT35 (Scanco Medical, Brüttisellen, Switzerland). 3D reconstruction and image visualization was performed using The Scanco micro-CT software (HP, DEC-windows Motif 1.6).

Biphasic Finite Element Model (bFEM)

Axisymmetric inhomogeneous biphasic finite element models (bFEM) were created as previously described.[10] Articular cartilage was modeled as a biphasic material with depth-dependent material properties.[19] Aggregate modulus, H_A, was input as a third-order polynomial function from the surface to the depth of the tissue, as follows[20]:

$$H_A = \left(3.794 \times \beta^3 - 0.646 \times \beta^2 + 1.777 \times \beta + 0.203\right) \times 0.69$$

Where $\alpha = 1-z/h$, z is vertical axial and h is cartilage thickness. This function approximates the depth-dependent properties in the immature bovine cartilage.[21] Permeability was input as $3 \times 10^{-15} m^4/Ns$ and Poisson's Ratio was 0.018.[22] Porous PVA was modeled as a biphasic homogeneous material and the confining ring was modeled as an elastic material. The model was designed to mimic the mechanical conditions at the start of loading (i.e., D28): material properties of the PVA scaffolds at D28 were measured by stepwise unconfined stress relaxation tests at strains of 4%, 8%, 12%, and 16%, using an EnduraTEC ELF 3200 system (Bose, Eden Prairie, MN).[23] Scaffold Aggregate Modulus, H_A was0.05 MPa, and Permeability was $2 \times 10^{-11} m^4/Ns$. The confining ring properties were $H_A = 0.971$ MPa and Poisson's ratio of 0.1. The scaffold-cartilage interface was modeled as friction contact with cohesion sliding resistance. Interface strength was quantified from D28 samples (Table 1, "inputs" column). Sinusoidal loading cycles of 1N and 6N were applied at 0.5 Hz to the surface of the simulated confined and unconfined constructs to result in four groups, as follows:

1. Unconfined, 1N load
2. Unconfined, 6N load
3. Confined, 1N load
4. Confined, 6N load

Equilibrium was reached when the displacement of the loading plate varied less than 0.5% between consecutive cycles,[10] at which stage (150 cycles) the simulation was stopped. The mechanical discontinuity at the interface was calculated as: peak micromotion, peak compressive stress, and peak principal shear stress at the scaffold-cartilage interface at the final cycle of loading.

Statistical Analysis

Statistical analysis was performed using GraphPad Prism software (La Jolla, CA). Two-way ANOVA was used for push-out stress and biochemical content as the dependent variables with culture condition (loads and boundary conditions) as independent variables. Bonferroni post-test analyses was performed with $\alpha = 0.05$ to consider statistical significance. All data are presented as mean ± SEM of $n = 10–12$ samples per group. Multivariate regression was performed using Systat SigmaPlot (v13, San Jose CA). The independent variables were the interface strength at the commencement of loading, the magnitude of the discontinuity across the interface in peak compressive stress and principal shear stress, scaffold peak compressive stress, and scaffold peak fluid shear stress (Table 1). The dependent variable was the output from physical bioreactor model (interface strength). Both forward and backward stepwise regression analyses were performed to verify the regression model.

RESULTS

Scaffold-Cartilage Integration

After 28 days of static culture, the confined samples had significantly higher interface strength when compared to the unconfined samples, while no difference was found after 42 days of static culture (0N), Fig. 2. The application of loads of 1N and 6N resulted in the confined samples having a significantly higher interfacial strength compared to the unconfined samples. The confined group with 1N of loading had significantly higher interfacial strength (50.2 ± 1.6 kPa) compared to all other groups (Fig. 2). The unconfined group had a significant decrease in interface strength at 1 and 6N of load compared to the static group at 42 days.

Biochemical Analysis of PVA Scaffolds: Scaffold GAG Content

After 28 days of static culture there was no significant differences in GAG content between the confined and unconfined samples (Fig. 3A), while after 42 days of static culture, the confined samples had significantly higher GAG content. The application of load at 1N and 6N resulted in the confined samples having a significantly higher GAG content compared to the unconfined samples. The highest GAG content (42.9 ± 1.1 μg, Fig. 3A) occurred in the confined group with 1N load.

Scaffold Collagen content: After 28 and 42 days of static culture, no differences were found in collagen content between the confined and unconfined samples (Fig. 3B). The application of 1N of load to unconfined samples resulted in significantly increased collagen content compared to day 28 static culture (Fig. 3B). Similarly, for confined samples mechanical loading at 6N significantly increased collagen content of scaffolds compared to the 28 and 42 day static culture groups (Fig. 3B). Of note, confining the specimens resulted in an increase in scaffold GAG content for each condition, but did not result in an increase in collagen content.

DNA content: DNA content was significantly higher in the confined group at 1N at D42 compared to that at D28 (Fig. 3C).

bFEM Results: Micromotion, Stresses, and Strains Within the PVA and Cartilage

At 1N of applied load, vertical displacements for the confined and unconfined conditions were homogeneous throughout the depth of the scaffold-cartilage constructs, ranging from 0 to 40 microns (Fig. 4A). At 6N of applied load, the distribution of vertical displacement for confined and unconfined conditions was inhomogeneous through the depth of the cartilage-scaffold construct: the superficial zone of the articular cartilage experienced higher vertical displacements than the deep zones. As expected, higher applied forces result in higher compressive stresses within the PVA and articular cartilage. For the confined and unconfined conditions at 1N of applied load, compressive stress was homogeneously distributed throughout the scaffold and cartilage, close to 0 kPa within the scaffold and 30–35 kPa within the articular cartilage (Fig. 4B). However, at 6N of applied load, the distribution of compressive stress throughout the articular cartilage was inhomogeneous, ranging from 40 to 160 kPa, while the distribution throughout the scaffold remained homogenous, ranging from 40 to 50 kPa (Fig. 4B). Peak Fluid Shear Stress: Increasing applied load from 1N to 6N resulted in an increase in peak fluid shear stress in the scaffold, 2–5 Pa in unconfined and 68–372 Pa in confined conditions (Table 1).

Mechanical Discontinuities at the Interface

At the interface between the scaffold and articular cartilage a discontinuity was identified in the compressive stress and shear stress for all conditions. Specifically, a discontinuity in the magnitude of compressive stress at mid-thickness ranged from a minimum of 20 kPa (1N, C) to a maximum of 154 kPa (6N, U), Fig. 4C and Table 1. The compressive and shear stress discontinuities were lowest in the 1N groups, irrespective of whether or not the groups were confined or unconfined. For all loading conditions, continuity in the magnitude of vertical displacement in a radial direction through each scaffold-cartilage construct was evident (Fig 4A). This situation resulted in no relative micromotion between the scaffold and cartilage at the interface throughout the depth of the constructs.

Histological and Micro-CT Analysis of Scaffold-Cartilage Integration

Two groups were chosen for microCT and histological analysis, (i) D42 1N confined (*the group that showed the highest push-out strength)* and (ii) D42 6N confined group. The bottom regions of the scaffolds of both groups displayed high GAG staining (Fig. 5A as indicated by arrows) compared to the lower regions, possibly due to cell sedimentation during the cell-seeding process. The 1N confined group had strong GAG staining at scaffold-cartilage interface, while disruption at the top of the interface of the 6N confined group was detected. A stronger and more uniform of collagen type II staining was also observed in 1N confined compared to 6N confined group (Fig. 5B). The micro-CT analysis and 3D reconstruction of 1N confined sample showed that the gap between scaffolds and the articular cartilage explant was completely filled after 42 days of culture (Fig. 5C), which corresponded to strong GAG staining at scaffold-cartilage interface. Conversely, the 6N confined exhibited a less physically connected interface and only partial gap filling.

Regression analysis identified that interface strength, prior to the commencement of loading (i.e., at Day 28), and peak fluid shear stress within the scaffold, created during loading, were responsible for 70.6% (Adj R^2) of the variation in the interface strength after 42 days of

culture. The coefficients were 1.356 for interface strength at D28: as interface strength at the commencement of loading increased, so too did the final interface strength. While the coefficient for the peak fluid shear stress within the scaffold was −0.0349 suggesting a weak inverse relationship between fluid shear stress and final interface strength, Table 2.

DISCUSSION

The objective of this study was to characterize how the mechanical environment within a scaffold-cartilage construct relates to lateral integration. We hypothesized that the magnitude of the mechanical discontinuity at the scaffold-cartilage interface would be related to decreased scaffold-cartilage integration. To test this hypothesis, we subjected cartilage-scaffold explants to a range of loading conditions by varying applied force, and peripheral confinement. Stress, strain, fluid flow, and displacements at the cartilage-scaffold interface and throughout the scaffold were quantified by computational inhomogeneous bFEMs. Interface strength, and scaffold collagen, GAG, and DNA content were quantified after 28 days of bioreactor loading. By applying multivariate regression analyses to compare the outputs from the computational model to the physical bioreactor model, we found that the strength of the interface prior to the commencement of loading and the shear stresses generated within the scaffold during loading were the main factors associated with integration.

As the variety of scaffolds suggested for cartilage repair continues to expand,[24,25] so do the number of design variables that can be chosen within each material combination: Morphology, modulus, permeability, porosity, for example.[26] A similarly broad number of techniques aimed at enhancing the scaffold-cartilage interface have been explored in vitro, including the use of nanofibers,[27] enzymatic digestion,[4,28] and adhesive factors.[7] While many of these options have shown promise in laboratory settings, the models used so far have not included mechanical loading, and instead have focused on static culture analyses. This omission is a critical flaw in efforts to translate technologies for cartilage repair to clinical use in joints that can experience contact stresses that range from 1 to 8 MPa during activities of daily living.[29,30] And yet, it is challenging to design bioreactor systems to mimic the stresses on cartilage during physiological activities.[31] For this reason, bioreactor systems, which can apply controlled axial forces[10,32,33] or controlled displacements/translations[34] to specimens are used.

It has been previously found that compressive loading has positive effects on collagen synthesis, as demonstrated by the up-regulation of *Col2a1* gene in mice chondrocytes cultured in agarose hydrogel, whereas the *Acan* gene encoding the protogylcan (aggrecan) was progressively decreased.[35] Another study demonstrated mechanical loading increased both GAGs and hydroxyproline contents of cell-seeded agarose hydrogel compared to free-swelling group up to 21 days.[36] But since these studies lack a mechanical analysis of hydrogel-cartilage interface mechanics, a direct analysis of the mechanical mechanisms driving the response at the interface has not been conducted. Moreover, the usefulness of parametric studies in which the profile, magnitude, frequency, rest period between loading bouts, and duration of application of load are varied,[36–38] but a mechanical analysis of the interface is omitted, is of questionable usefulness.

It is challenging, if not impossible, to directly control mechanical conditions along scaffold-cartilage interfaces in bioreactor systems. Therefore, in this study, we sought to indirectly control interface mechanics by altering peripheral confinement and the magnitude of applied load. By applying a computational model, in this case a bFEM to the analysis of specific bioreactor loading and boundary conditions, the mechanical environment within the loaded construct and at the interface between the cartilage and scaffold can be quantified. FE models have been used to quantify the micro-mechanical environment of chondrocytes within mechanically loaded tissue,[39] and from the nucleus to the pericellular and extracellular matrix.[40] By mimicking the biphasic characteristics of articular cartilage, an analysis of the fluid flow around the cell and through the matrix is possible.[12] For the current study, the bFEM developed was used to quantify tissue mechanics across a range of loading and peripheral confinement conditions, to parallel the physical bioreactor model.

For all loading and boundary conditions, compressive and shear stress mechanical discontinuities were found at the scaffold-cartilage interface, the magnitude of which was higher in the 6N group for the confined and unconfined conditions. Of note, a displacement discontinuity at the interface was not identified. Compressive stresses within the scaffold were also higher in the 6N confined and unconfined groups; while peak fluid shear stresses *within* the scaffold were higher for the confined group and 5-fold higher for 6N versus 1N of applied load. An unintended consequence of the variation in confined or unconfined peripheries was that peripheral confinement during static culture resulted in a twofold increase in initial scaffold-cartilage interface strength, prior to the application of bioreactor loads. This finding is similar to that reported for peripherally confined cell seeded hydrogels, [41] and was reflected in the inputs to the bFEMs. We previously applied a similar combined bFEM/bioreactor system to the analysis of scaffold-cartilage integration[10] and identified more extreme mechanical discontinuities at the scaffold-cartilage interface, which included scaffold-cartilage micromotion of up to 200 microns. While similarities existed between both studies (identical scaffolds and pre-incubation times were used), the scaffolds in the Chen et al.,[10] study were not pre-seeded with cells and, as such, the strength of the interface at the commencement of loading was substantially lower than that of the cell-seeded scaffolds used in the current study. When taken together, both the previous and the current study suggest the existence of a minimum level of scaffold-cartilage integration required prior to the commencement of loading, although the exact minimum threshold has yet to be identified.

A unique aspect to our study was the comparison of the mechanical conditions quantified using the bFEM within the scaffold-cartilage construct, to the mechanical strength of the interface and the biochemical contents within the scaffold. Loading, particularly at 1N, in peripherally confined specimen resulted in a significant increase in scaffold sGAG, DNA content, and scaffold-cartilage interface strength. An important finding is that the multivariate regression analysis identified that scaffold-cartilage integration was not affected by the extent of the mechanical discontinuity, but rather is influenced by strength of the scaffold-cartilage interface at the commencement of loading, and weakly affected by the magnitude of the peak fluid shear stresses within the scaffold. When taken in conjunction with the results of Chen et al.,[42] the need for an, as yet indeterminate, degree of integration

prior to the application of load is clear. This result has important clinical implications, as rehabilitation protocols for cartilage repair technologies remain under development.

Our results further point to the concept of “stress shielding” where load follows stiffness, and can lead to under-loading situations; a phenomena most commonly discussed in the context of arthroplasty.[43] In the case of scaffold-cartilage integration, for example, consider a low modulus scaffold implanted into a high modulus rim of articular cartilage. When loaded, force will preferentially get distributed through the higher modulus rim, and in doing so will prevent the cells within the scaffold from experiencing the mechanical stimulus required for them to lay down matrix. But, as the scaffold becomes integrated with the host tissue, and its modulus increased, there is more opportunity for loads to be distributed through the scaffold and stimulate the continued cells. While a more detailed parametric study is required to fully explore this relationship, this study points to the fact that multiple and interconnecting mechanical factors affect the integrity of the scaffold-cartilage interface.

Our study had limitations. Once initial integration occurred, which in our case was at D28, the strength of the interface over time can be influenced by many factors. For example, if interfacial stresses exceed the strength of the matrix that has formed, mechanical disruption of that matrix can occur.[44] In another scenario, mechanical stresses at that interface can be stimulatory[45] and encourage interface cells to lay down matrix, or may inhibit biological activity.[44,46,47] Our study did not identify these contrasting scenarios. To facilitate the combined computational-bioreactor approach, we utilized a non-degradable porous scaffold, PVA, which avoids the complexity of modeling the changing environment of degradable scaffolds in the bFEM.[26,48] The use of non-degradable materials for cartilage repair/replacement remains controversial, and at times has been suggested more suitable for older patients, with limited tissue regenerative capacity.[49] The porous PVA formulation used herein combines some of the advantages of non-degradable materials[50]—maintaining a minimum amount of material to withstand load, while also providing the ability to integrate with articular cartilage in both loaded and unloaded explant models,[28] but the results of our study cannot be directly extrapolated to rapidly degrading scaffolds. Finally, dues to challenges in histological processing, especially PVA constructs with low levels of integration, histological analysis was restricted to two groups.

In summary, using parallel computational and physical bioreactor models in which the applied loading and peripheral confinement were controlled, we were able to identify compressive and shear stress mechanical discontinuities at the scaffold-cartilage interface, the magnitude of which could be varied by controlling the pre-incubation conditions, peripheral confinement, and applied load. Our hypothesis was rejected: the magnitude of the mechanical discontinuity (shear stress, compressive stress, micromotion) at the scaffold-cartilage interface was not solely associated with reduced scaffold-cartilage integration. Rather, the strength of the interface prior to the commencement of loading and the shear stresses generated within the scaffold during loading were the main factors associated with physical integration.

ACKNOWLEDGMENTS

Research reported in this publication was supported by NIAMS of the National Institutes of Health under award number R01AR066635. Support was also provided by the Widgeon Charitable Foundation and the Russell Warren Chair of Tissue Engineering.

REFERENCES

1. Sophia Fox AJ, Bedi A, Rodeo SA. 2009 The basic science of articular cartilage: structure, composition, and function. Sports Health 1:461–468. [PubMed: 23015907]
2. Davies LC, Blain EJ, Caterson B, et al. 2008 Chondroitin sulphate impedes the migration of a sub-population of articular cartilage chondrocytes. Osteoarthritis and cartilage/OARS. Osteoarthritis Res Soc 16:855–864.
3. Knudson W, Casey B, Nishida Y, et al. 2000 Hyaluronan oligosaccharides perturb cartilage matrix homeostasis and induce chondrocytic chondrolysis. Arthritis Rheum 43:1165–1174. [PubMed: 10817571]
4. Obradovic B, Martin I, Padera RF, et al. 2001 Integration of engineered cartilage. J Orthop Res 19:1089–1097. [PubMed: 11781010]
5. Khan IM, Gonzalez LG, Francis L, et al. 2011 Interleukin-1beta enhances cartilage-to-cartilage integration. Eur Cells Mater 22:190–201.
6. Freed LE, Grande DA, Lingbin Z, et al. 1994 Joint resurfacing using allograft chondrocytes and synthetic biodegradable polymer scaffolds. J Biomed Mater Res 28:891–899. [PubMed: 7983087]
7. Allon AA, Ng KW, Hammoud S, et al. 2012 Augmenting the articular cartilage-implant interface: functionalizing with a collagen adhesion protein. J Biomed Mater Res Part A 100:2168–2175.
8. Moutos FT, Freed LE, Guilak F. 2007 A biomimetic three-dimensional woven composite scaffold for functional tissue engineering of cartilage. Nat Mater 6:162–167. [PubMed: 17237789]
9. Waldman SD, Spiteri CG, Grynpas MD, et al. 2003 Long-term intermittent shear deformation improves the quality of cartilaginous tissue formed in vitro. J Orthop Res 21:590–596. [PubMed: 12798056]
10. Chen T, McCarthy MM, Guo H, et al. 2018 The scaffold-articular cartilage interface: a combined in vitro and In silico analysis under controlled loading conditions. J Biomech Eng 140 10.1115/1.4040121
11. Vahdati A, Zhao Y, Ovaert TC, et al. 2012 Computational investigation of fibrin mechanical and damage properties at the interface between native cartilage and implant. J Biomech Eng 134:111004. [PubMed: 23387786]
12. Khoshgoftar M, Torzilli PA, Maher SA. 2018 Influence of the pericellular and extracellular matrix structural properties on chondrocyte mechanics. J Orthop Res 36:721–729. [PubMed: 29044742]
13. Ng KW, Torzilli PA, Warren RF, et al. 2014 Characterization of a macroporous polyvinyl alcohol scaffold for the repair of focal articular cartilage defects. J Tissue Eng Regen Med 8:164–168. [PubMed: 22549901]
14. Ng KW, Wanivenhaus F, Chen T, et al. 2012 A novel macroporous polyvinyl alcohol scaffold promotes chondrocyte migration and interface formation in an in vitro cartilage defect model. Tissue Eng Part A 18:1273–1281. [PubMed: 22435602]
15. Byers BA, Mauck RL, Chiang IE, et al. 2008 Transient exposure to transforming growth factor beta 3 under serum-free conditions enhances the biomechanical and biochemical maturation of tissue-engineered cartilage. Tissue Eng Part A 14:1821–1834. [PubMed: 18611145]
16. van de Breevaart Bravenboer J, In der Maur CD, Bos PK, et al. 2004 Improved cartilage integration and interfacial strength after enzymatic treatment in a cartilage transplantation model. Arthritis Res Ther 6:R469–R476. [PubMed: 15380046]
17. Farndale RW, Sayers CA, Barrett AJ. 1982 A direct spectrophotometric microassay for sulfated glycosaminoglycans in cartilage cultures. Connective Tissue Res 9:247–248.
18. Reddy GK, Enwemeka CS. 1996 A simplified method for the analysis of hydroxyproline in biological tissues. Clin Biochem 29:225–229. [PubMed: 8740508]

19. Guo H, Maher SA, Torzilli PA. 2014 A biphasic multiscale study of the mechanical microenvironment of chondrocytes within articular cartilage under unconfined compression. J Biomech 47:2721–2729. [PubMed: 24882738]
20. Chen AC, Bae WC, Schinagl RM, et al. 2001 Depth- and strain-dependent mechanical and electromechanical properties of full-thickness bovine articular cartilage in confined compression. J Biomech 34:1–12. [PubMed: 11425068]
21. Bian L, Lima EG, Angione SL, et al. 2008 Mechanical and biochemical characterization of cartilage explants in serum-free culture. J Biomech 41:1153–1159. [PubMed: 18374344]
22. Mow VC, Gu WY, Chen FH. 2005 Structure and function of articular cartilage and meniscus In: Mow VC, Huiskes R, editors. Basic orthopaedic biomechanics and mechano-biology. Philadelphia: Lippincott p 181.
23. Awad HA, Wickham MQ, Leddy HA, et al. 2004 Chondrogenic differentiation of adipose-derived adult stem cells in agarose, alginate, and gelatin scaffolds. Biomaterials 25:3211–3222. [PubMed: 14980416]
24. Moutos FT, Guilak F. 2008 Composite scaffolds for cartilage tissue engineering. Biorheology 45:501–512. [PubMed: 18836249]
25. Kim IL, Mauck RL, Burdick JA. 2011 Hydrogel design for cartilage tissue engineering: a case study with hyaluronic acid. Biomaterials 32:8771–8782. [PubMed: 21903262]
26. Annabi N, Nichol JW, Zhong X, et al. 2010 Controlling the porosity and microarchitecture of hydrogels for tissue engineering. Tissue Eng Part B, Rev 16:371–383. [PubMed: 20121414]
27. Maher SA, Mauck RL, Rackwitz L, et al. 2010 A nanofibrous cell-seeded hydrogel promotes integration in a cartilage gap model. J Tissue Eng Regen Med 4:25–29. [PubMed: 19834956]
28. Ng KW, Wanivenhaus F, Chen T, et al. 2012 A novel macroporous polyvinyl alcohol scaffold promotes chondrocyte migration and interface formation in an in vitro cartilage defect model. Tissue Eng Part A 18:1273–1281. [PubMed: 22435602]
29. Wang H, Chen T, Torzilli P, et al. 2014 Dynamic contact stress patterns on the tibial plateaus during simulated gait: a novel application of normalized cross correlation. J Biomech 47:568–574. [PubMed: 24342497]
30. Bedi A, Kelly NH, Baad M, et al. 2010 Dynamic contact mechanics of the medial meniscus as a function of radial tear, repair, and partial meniscectomy. J Bone Joint Surg Am 92:1398–1408. [PubMed: 20516315]
31. Gilbert S, Chen T, Hutchinson ID, et al. 2014 Dynamic contact mechanics on the tibial plateau of the human knee during activities of daily living. J Biomech 47:2006–2012. [PubMed: 24296275]
32. Torzilli PA, Bhargava M, Park S, et al. 2010 Mechanical load inhibits IL-1 induced matrix degradation in articular cartilage. Osteoarthritis and cartilage/OARS. Osteoarthritis Res Soc 18:97–105.
33. Piscoya JL, Fermor B, Kraus VB, et al. 2005 The influence of mechanical compression on the induction of osteoarthritis-related biomarkers in articular cartilage explants. Osteoarthritis and cartilage/OARS. Osteoarthritis Res Soc 13:1092–1099.
34. Buschmann MD, Gluzband YA, Grodzinsky AJ, et al. 1995 Mechanical compression modulates matrix biosynthesis in chondrocyte/agarose culture. J Cell Sci 108:1497–1508. [PubMed: 7615670]
35. Wu P, DeLassus E, Patra D, et al. 2013 Effects of serum and compressive loading on the cartilage matrix synthesis and spatiotemporal deposition around chondrocytes in 3D culture. Tissue Eng Part A 19:1199–1208. [PubMed: 23410025]
36. Mauck RL, Soltz MA, Wang CC, et al. 2000 Functional tissue engineering of articular cartilage through dynamic loading of chondrocyte-seeded agarose gels. J Biomech Eng 122:252–260. [PubMed: 10923293]
37. Parkkinen JJ, Lammi MJ, Helminen HJ. 1992 Local stimulation of proteoglycan synthesis in articular cartilage explants by dynamic compression in vitro. J Orthop Res 10:610–620. [PubMed: 1500975]
38. Davisson T, Kunig S, Chen A, et al. 2002 Static and dynamic compression modulate matrix metabolism in tissue engineered cartilage. J Orthop Res 20:842–848. [PubMed: 12168676]

39. Klika V, Gaffney EA, Chen YC, et al. 2016 An overview of multiphase cartilage mechanical modelling and its role in understanding function and pathology. J Mech Behav Biomed Mater 62:139–157. [PubMed: 27195911]
40. Guo H, Torzilli PA. 2016 Shape of chondrocytes within articular cartilage affects the solid but not the fluid microenvironment under unconfined compression. Acta Biomaterialia 29:170–179. [PubMed: 26525115]
41. Thorpe SD, Nagel T, Carroll SF, et al. 2013 Modulating gradients in regulatory signals within mesenchymal stem cell seeded hydrogels: a novel strategy to engineer zonal articular cartilage. PLoS ONE 8:e60764. [PubMed: 23613745]
42. Edwards PK, Ackland T, Ebert JR. 2014 Clinical rehabilitation guidelines for matrix-induced autologous chondrocyte implantation on the tibiofemoral joint. J Orthop Sports Phys Ther 44:102–119. [PubMed: 24175609]
43. Velasco MA, Narvaez-Tovar CA, Garzon-Alvarado DA. 2015 Design, materials, and mechanobiology of biodegradable scaffolds for bone tissue engineering. Biomed Res Int 2015:729076. [PubMed: 25883972]
44. Bader DL, Salter DM, Chowdhury TT. 2011 Biomechanical influence of cartilage homeostasis in health and disease. Arthritis 2011:979032. [PubMed: 22046527]
45. Buschmann MD, Kim YJ, Wong M, et al. 1999 Stimulation of aggrecan synthesis in cartilage explants by cyclic loading is localized to regions of high interstitial fluid flow. Arch Biochem Biophys 366:1–7. [PubMed: 10334856]
46. Guilak F, Hung CT. 2005 Physical regulation of cartilage metabolism In: Mow VC, Huiskes R, editors. Basic orthopaedic biomechanics & mechano-biology. Philadelphia: Lippincott pp. 275–298.
47. Ng KW, Mauck RL, Wang CC, et al. 2009 Duty cycle of deformational loading influences the growth of engineered articular cartilage. Cell Mol Bioeng 2:386–394. [PubMed: 20703332]
48. Zhu Y, Jiang H, Ye SH, et al. 2015 Tailoring the degradation rates of thermally responsive hydrogels designed for soft tissue injection by varying the autocatalytic potential. Biomaterials 53:484–493. [PubMed: 25890745]
49. Jeuken RM, Roth AK, Peters RJRW, et al. 2016 Polymers in cartilage defect repair of the knee: current status and future prospects. Polymers-Basel 8.
50. Spiller KL, Maher SA, Lowman AM. 2011 Hydrogels for the repair of articular cartilage defects. Tissue Eng Part B-Re 17:281–299.

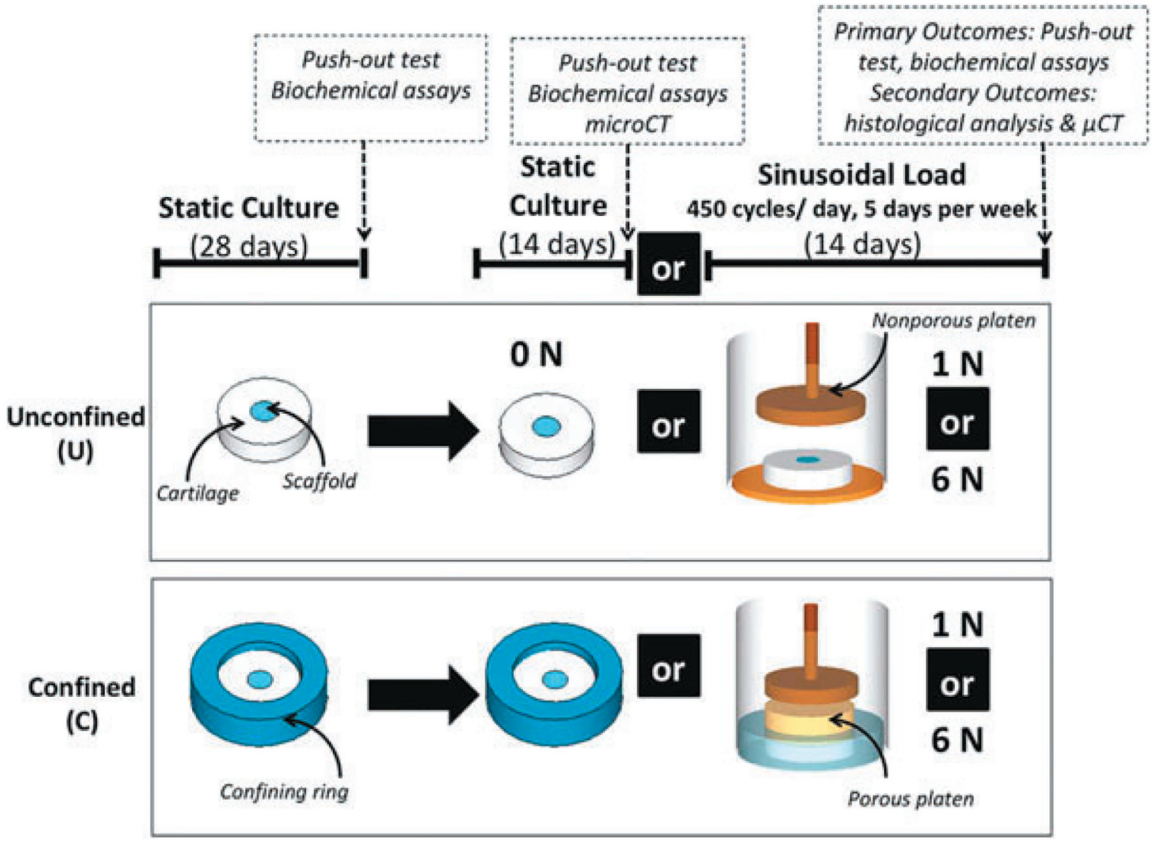

Figure 1.

Experimental design of bioreactor physical model: Scaffold-cartilage constructs were cultured under unconfined conditions (U), or peripherally confined conditions (C) for 28 days. Constructs were then subjected to either continued static culture (0 N), or a sinusoidal load of 1 N or 6 N, applied at 0.5 Hz once every day for 450 cycles for 5 days per week for 14 days.

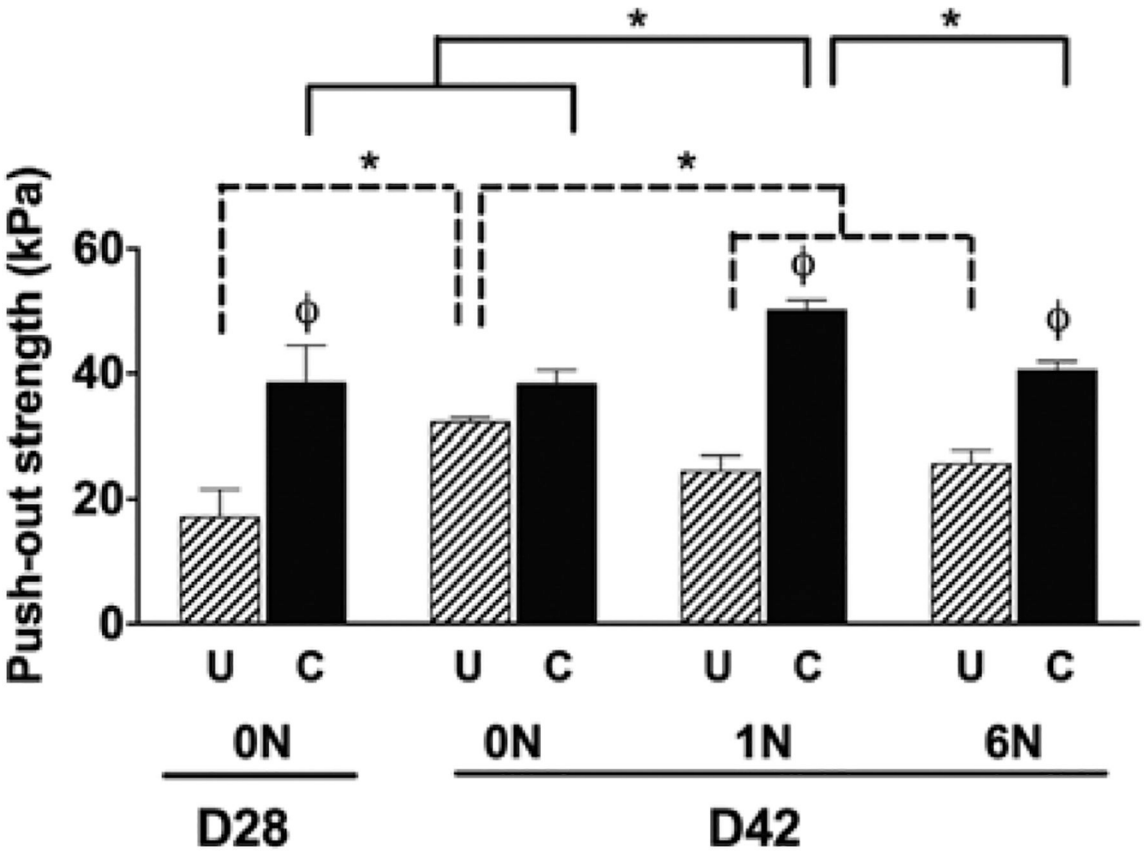

Figure 2.

Maximum push-out stress (kPa) as physically quantified at the end of static culture (D28) and after 14 days of no loading (0N), loading (1N and 6N) for unconfined (U) conditions and confined conditions (C) Data show average ± SEM of $n = 12$. ϕ indicates significant effects of boundary condition/confinement. * Indicates significant effects of loading.

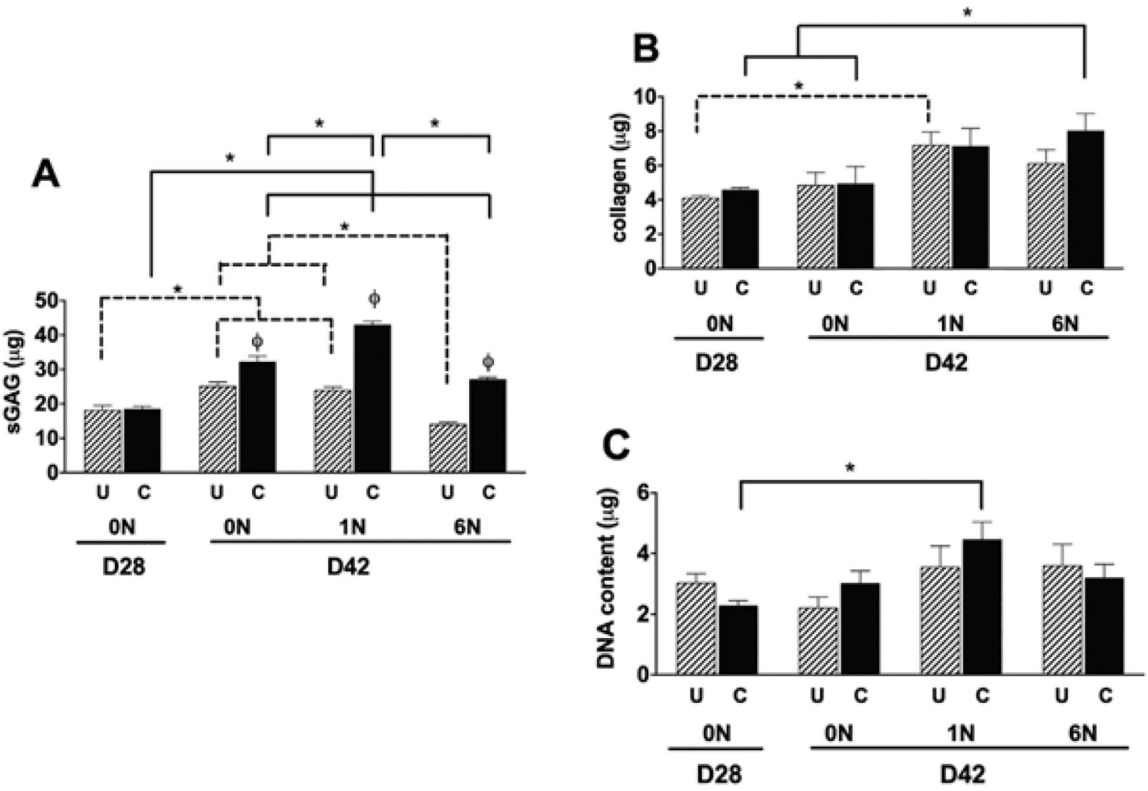

Figure 3.

Biochemical content of PVA scaffolds: PVA scaffolds were analyzed for Glycosaminoglycan (GAG) (A) collagen (B) and DNA (C) content. Data show average ± SEM of $n = 12$. ϕ indicates significant effects of boundary condition/confinement * Indicates significant effects of loading.

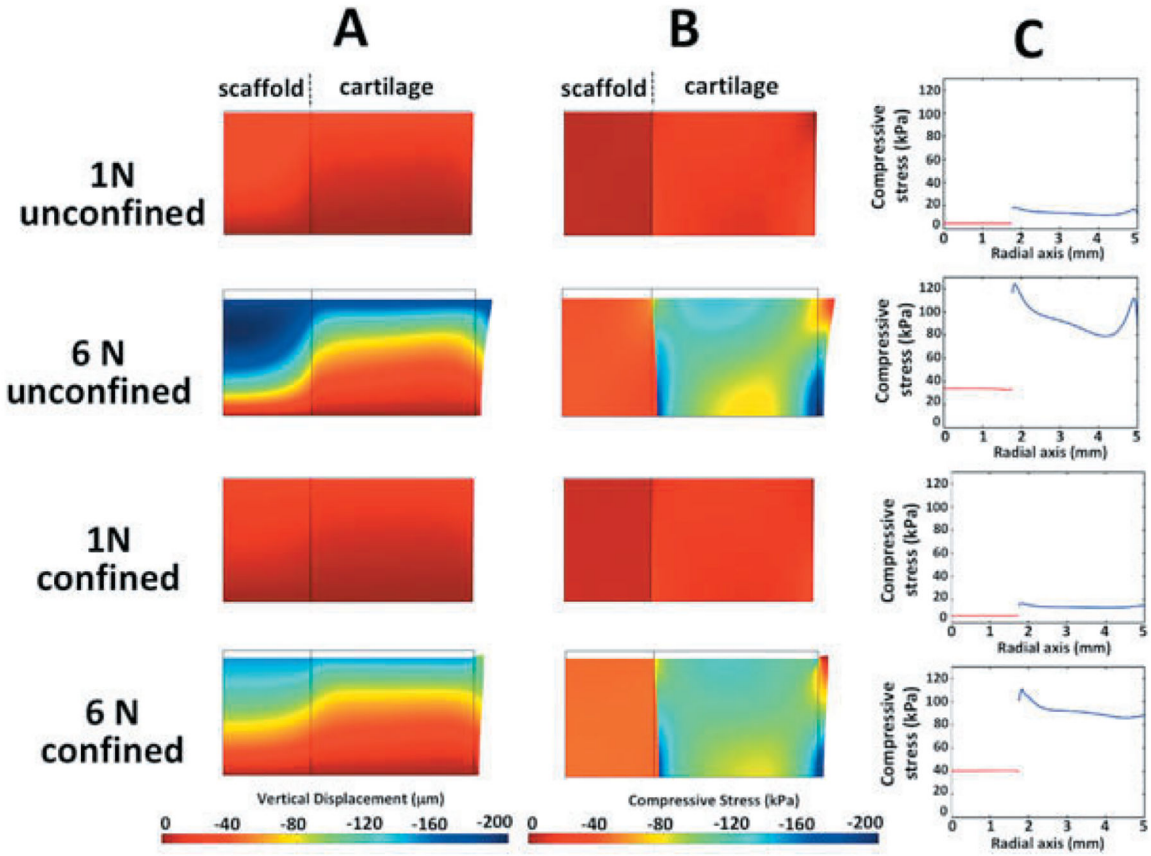

Figure 4.

Biphasic finite element models (bFEMs): (A) distribution of vertical displacement; (B) distribution of compressive stress; (C) compressive stress at mid-vertical height of the model, where red lines indicate scaffold and blue lines indicate cartilage, respectively.

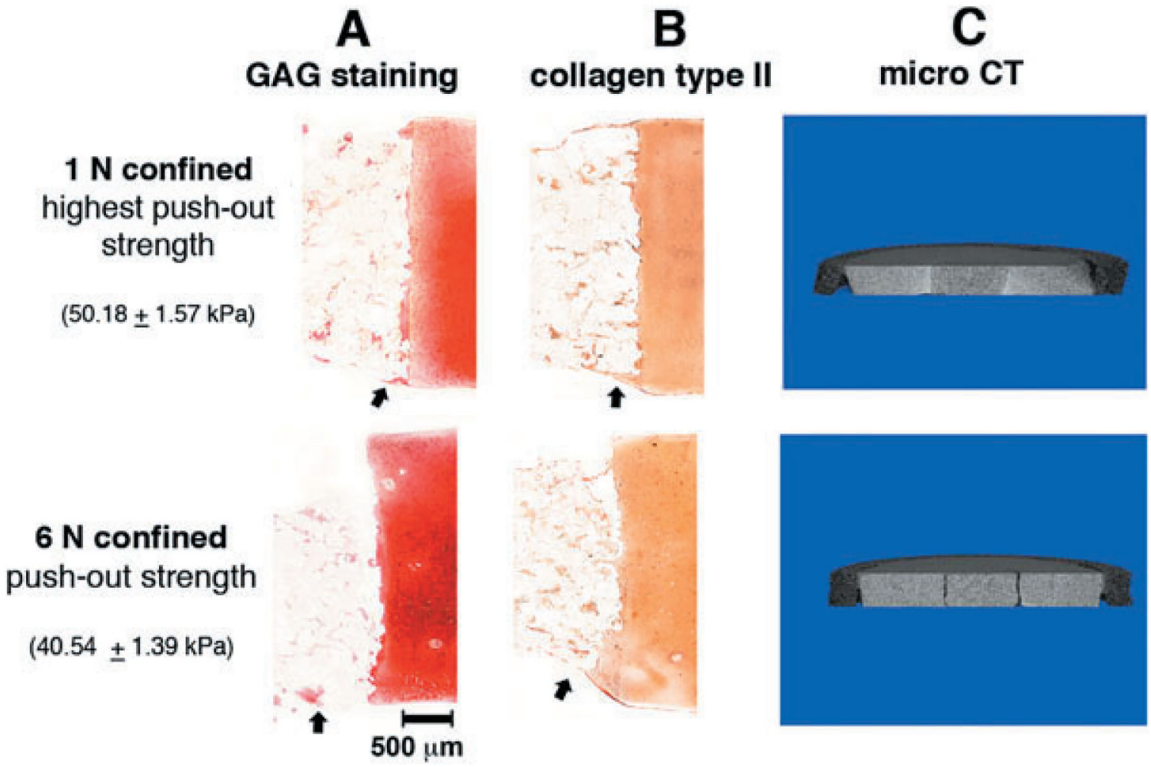

Figure 5.

Histology and microCT: GAG staining of PVA scaffold and cartilage (A); immunohistochemistry of collagen type II (B); and cross-section of 3D reconstruction of the defect model (C). Arrows indicate areas of matrix production at the scaffold-cartilage interface.

Table 1.

Summary Data From the Computational and Physical Models

Inputs to Computational Model		Outputs from Computational Model Discontinuity at the Interface		Outputs from Computational Model Scaffold Stresses		Outputs From Physical Bioreactor at D42
Loading Conditions	**Interface Strength at D28 (kPa)**	**Peak Compressive Stress (kPa)**	**Principal Shear Stress (kPa)**	**Peak Compressive Stress (kPa) in PVA**	**Peak Fluid Shear Stress (Pa) in PVA**	**Interface Strength at D42 (kPa)**
1 N, U	17.4	23	27	5	2	24.54±2.52
6 N, U	17.4	154	179	34–160	5	25.66±2.29
1 N, C	38	20	23	6	68	50.18±1.57
6 N, C	38	134	156	40–160	372	40.54±1.39

Table 2.

Variables in Multivariate Regression Model: The Analysis of Variance from the Multivariate Regression Model Had a p value <0.001 and an Adj R^2 = 0.706

Variables in Model	Coeff.	Std. Coeff.	Std. Error	*P* Value
Constant	1.598	–	5.058	–
D28 interface strength	1.356	1.118	0.214	<0.001
Peak fluid shear stress PVA	−0.0349	−0.431	0.0125	0.007